Astron. Astrophys. 320, 249–256 (1997)

ASTRONOMY AND ASTROPHYSICS

Superwind in evolved OH/IR stars

X. Delfosse[1], **C. Kahane**[1], **and T. Forveille**[1]

Observatoire de Grenoble, B.P. 53, F-38041 Grenoble Cedex 9, France
(delfosse@gag.observ-gr.fr; kahane@gag.observ-gr.fr; forveill@gag.observ-gr.fr;)

Received 22 July 1996 / Accepted 13 September 1996

Abstract. We report observations of ^{13}CO (J=1–0) and (J=2–1) emission towards 5 evolved OH/IR envelopes. Four of them are known to have very weak CO emission compared to their infrared flux, and an anomalously high (J=2–1)/(J=1–0) intensity ratio. Modeling of their ^{12}CO and ^{13}CO lines is used to test several possible explanations of this behaviour. We conclude that it is most likely due to the recent onset of a superwind phase. Another interesting result of the modeling is the very low ^{12}C/^{13}C isotopic ratios we derive in these envelopes, of the order of 3.5 and close to the equilibrium value of the CNO cycle. We interpret this as the signature of massive stars at the end of their AGB phase. The sixth envelope, which shows a much lower (J=2–1)/(J=1–0) intensity ratio, also has a low, marginally larger, ^{12}C/^{13}C isotopic ratio. We conclude that it also is a massive object, but in a slightly less evolved stage, just before the superwind phase.

Key words: stars: circumstellar matter – stars: AGB, post-AGB – stars: mass loss – radio lines: stars

1. Introduction

Mass loss from AGB giants is important both in the evolution of the star and for the replenishment of the interstellar medium. Derivation of AGB mass loss rates relies on essentially two methods: (i) radio observations of their molecular gas (mainly CO) in the circumstellar shell, which provide measurements of both the gas expansion velocity and the mass loss rate and (ii) infrared observations of the circumstellar dust (e.g. van der Veen & Olofsson, 1990).

Towards optically visible Mira variables and carbon stars, the CO line intensities are well correlated with the infrared fluxes and the derivation of the star's mass loss rate from various data (CO(1–0) or CO(2–1) intensities, infrared emission) provides consistent values.

For the optically thick OH/IR stars in contrast, mass loss rates derived from dust and molecular gas emission often differ by orders of magnitude (Heske et al., 1990, hereafter HFOVH). Based on CO(J=1–0) and CO(J=2–1) observations of 13 OH/IR envelopes, HFOV have classified the OH/IR stars in two groups. The less opaque envelopes have relatively low mass loss rates ($\dot{M} \leq 10^{-5}$ M$_\odot$ yr^{-1}), consistently derived from 60 μm flux and from ^{12}CO emission. In this subsample, the ^{12}CO (J=2–1)/(J=1–0) integrated intensity ratio is ~ 2, as in the less opaque Mira and carbon star envelopes. The OH/IR stars with the thickest envelopes have weak CO emission compared to their infrared fluxes: their mass loss rates derived from IR emission (HFOVH, Justtanont & Tielens, 1992; Justtanont et al., 1996) are an order of magnitude higher ($\dot{M} \sim 10^{-4}$M$_\odot$ yr^{-1}) than for the less opaque OH/IR stars, while those derived from CO are similar. In these thicker envelopes, the ^{12}CO (J=2–1)/(J=1–0) integrated intensity ratio is ~ 4.

Two interpretations of this molecular/dust mass loss discrepancy have been proposed by HFOVH (and subsequently discussed by various authors): a cold outer envelope and a recent mass loss increase. We test them here through radiative transfer models of the ^{12}CO (J=2–1) and (J=1–0) lines in six OH/IR stars observed by HFOVH. In addition, we use new observations of ^{13}CO emission from five OH/IR stars (four of which are "CO deficient" envelopes) to derive their ^{12}C/^{13}C isotopic ratio, a sensitive probe of stellar evolution along the AGB.

In Sect. 2. we describe the ^{13}CO observations, carried out with the IRAM 30m telescope. Sect. 3 briefly describes the radiative transfer program. In Sect. 4 we examine three alternative models of the CO emission towards the "prototype" cold OH/IR star, OH127.8-0.0. The most convincing model, that of a superwind, is then applied to the five other OH/IR stars in Sect. 5. The results, in particular the ^{12}CO/^{13}CO isotopic ratios, are discussed in terms of stellar evolution in Sect. 6.

2. Observations

The ^{13}CO observations were carried out in January 1991 with the IRAM 30m telescope. The telescope was equipped with SIS receivers. The antenna temperature scale was calibrated every 10 minutes, with the cold load technique. All antenna temperatures reported in this paper, including the system temperatures, are main beam averaged temperatures (T_{mb}). They are related

Send offprint requests to: X. Delfosse

Table 1. Antenna and receiver characteristics

Line	Frequency (MHz)	HPBW (")	B_{eff}	F_{eff}	T_{sys} (K)	ΔV (km s^{-1})
^{13}CO(1–0)	110201.4	21	0.61	0.90	500–700	2.72
^{13}CO(2–1)	220398.7	13	0.46	0.90	1500–2000	1.36

Table 2. ^{13}CO line parameters

OH	Line	$\int$ T$_{mb}$ dv (K.km.s^{-1})	v$_{LSR}$ (km.s^{-1})	v$_{exp}$ (km.s^{-1})
127.8-0.0	(1–0)	1.6 (0.2)	-50.9 (0.3)	14.9 (0.3)
	(2–1)	6.5 (0.4)	-54.8 (0.3)	11.7 (0.3)
30.1-0.7	(1–0)	3.3 (0.3)	103 (0.5)	17.7 (0.5)
	(2–1)	14.5 (0.6)	101 (0.7)	18.7 (0.7)
104.9+2.4	(1–0)	(0.8)	-	-
	(2–1)	3.3 (0.5)	-30.7 (1.2)	12.2 (1.2)
26.5+0.6	(2–1)	11.8 (1.9)	27.3 (0.8)	14.9 (0.8)
63.3-10.2	(1–0)	1.7 (0.3)	-73.0 (0.9)	13.4 (0.9)
	(2–1)	7.3 (0.6)	-71.8 (0.2)	16.8 (0.2)

Numbers in parenthesis are 1 σ error bars

to the effective single sideband antenna temperatures above the atmosphere, T_A^*, by T_{mb} = T_A^*/η where η is the ratio of the main beam to forward beam efficiencies (B_{eff} and F_{eff} respectively). The main antenna and receiver characteristics are reported in Table 1.

The observations were made in position-switching mode, with a reference position 120" east of the star position. Pointing was checked every hour on planets and remained accurate to about 3 arcsec rms. Typical integration times were 20 to 40 minutes, corresponding to rms noises in 1-MHz channels of $\sim$ 0.03 K for the (1–0) spectra and $\sim$ 0.07 K for the (2–1) spectra. The spectra are plotted in Figs. 1 and 2, together with the ^{12}CO spectra of HFOVH.

The integrated intensities, central velocities and expansion velocities reported in Table 2 are derived from a fit of the observed lines with model profiles (truncated parabola) corresponding to uniformly expanding spherical shells (numbers in parenthesis are 1 σ error bars). The detection of the ^{13}CO(2-1) line for OH104.9+2.4 is marginal.

3. The model

We have modeled the CO lines using a radiative transfer code developed by Robert Lucas for spherically symmetric circumstellar envelopes. The same program was used by Kahane & Jura (1994) who discussed it in some detail. Briefly, this program computes the level populations throughout the envelope using the Sobolev approximation, and then solves the exact radiative transfer equation to derive the emergent line profiles. It takes into account CO excitation by the cosmic background radiation, by infrared radiation from the central star, and by collisions with H_2 (with collisional cross sections from Schinke et al. (1985)).

Table 3. Adopted distances and expansion velocities

OH	Distance (pc)	V$_e$ (km/s)
127.8-0.0	2900	13.0
30.1-0.7	2100	20.2
104.9+2.4	2300	15.5
26.5+0.6	1440	13.9
138.0-7.3	3400	9.5
63.3-10.2	2600	16.4

We have included 15 rotational levels for each of the first two vibrational levels of the CO molecule, and checked that the results for the observed transitions were unaffected when including more levels. Since collisions dominate the CO rotational excitation in the thick envelopes of OH/IR stars, the accuracy of the infrared radiation field is not critical. We have simply assumed that the observed IR flux, between 1μm and 100μm, (taken from the compilation of Gezari et al., 1987) is emitted by a central point source. The adopted CO abundance relative to H_2 is 3×10^{-4}, apropriate for oxygen rich circumstellar envelopes (see, for example, Knapp & Morris (1985)). The expansion velocities were derived from the ^{12}CO profiles. Their values are listed in Table 3, together with the adopted stellar distances.

Whenever possible these are phase lag distances from Van Langevelde et al. 1990, or from Herman & Habing (1985) for OH138.0-7.3. For OH30.1-0.7 and OH63.3-10.2, they had to be derived from the assumption of a standard value for the bolometric luminosity (10^4L$_\odot$, see HFOVH). The model brightness temperatures were converted to main beam brightness temperatures assuming a gaussian beam with the measured HPBW of the 30m telescope (12.5" for ^{12}CO(2–1), 20" for ^{12}CO(1–0), 13" for ^{13}CO(2–1) and 21" for ^{13}CO(1–0)). The remaining model parameters are the kinetic temperature radial dependence, the mass loss rate and the isotopic abundance ratio ^{12}CO/^{13}CO. They are the quantities we intend to constrain.

4. Modeling ^{12}CO and ^{13}CO emissions from OH127.8-0.0

Among the four heavily obscured OH/IR stars in Table 2, only OH127.8+0.0 and OH30.1-0.7 have measurements of the J=2–1 and J=1–0 transitions for both isotopes. Since emission from OH30.1-0.7 is more affected by an interstellar contribution, we consider OH127.8+0.0 in detail here, and use it as the testing-bench for various models.

As first mentioned by HFOVH, all models of CO emission from a constant mass loss rate circumstellar envelope with a standard temperature law fail to reproduce the observed (2–1)/(1–0) intensity ratios ($\sim$ 4) in heavily obscured OH/IR stars. Such high ratios require that the outer layers of the envelope, which are likely to contribute more to the (1–0) transition than to the (2–1) transition, do not contribute at all to CO emission.

Various ways of producing this effect have been suggested in the literature and we will consider them in turn, starting with those which can be easily ruled out.

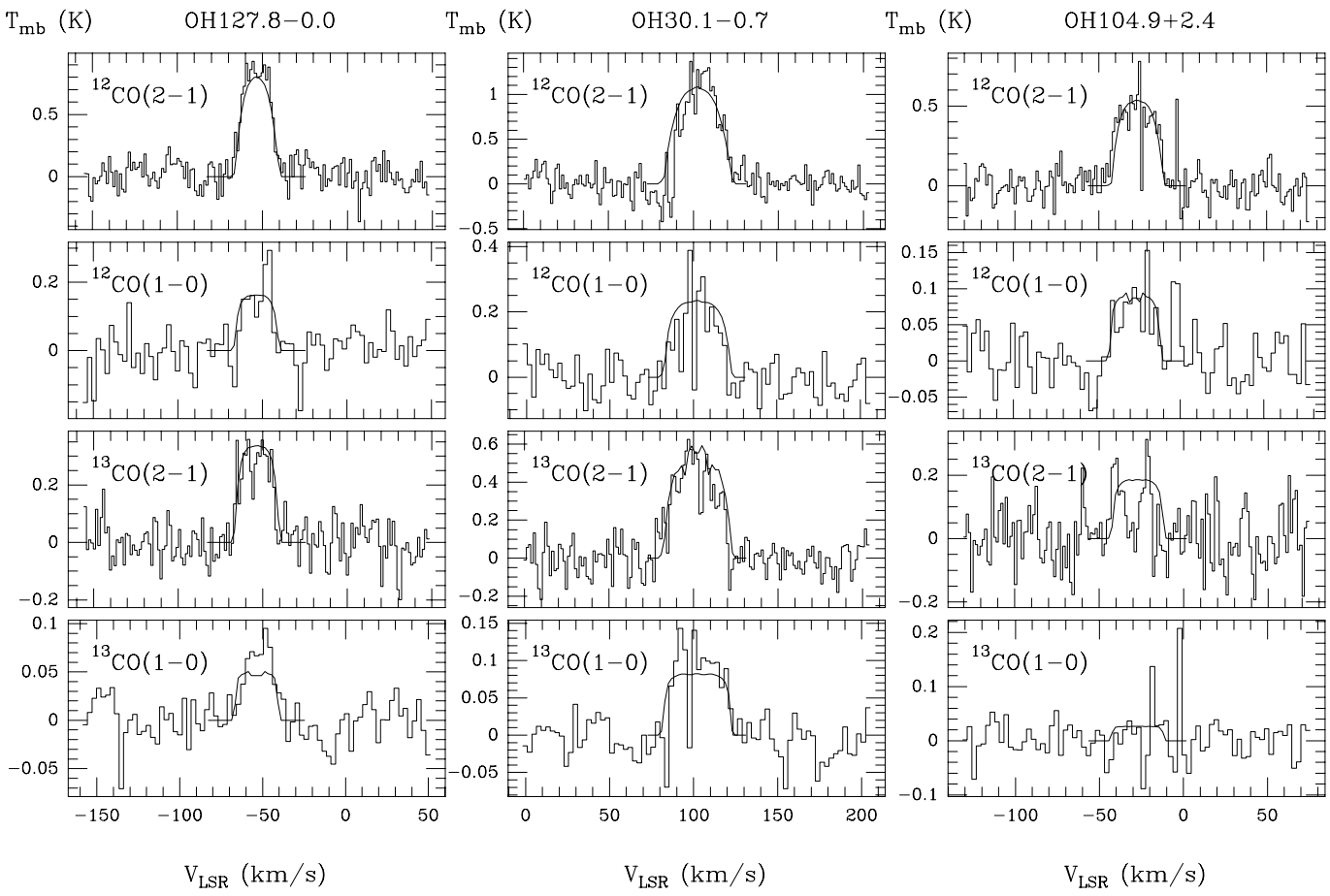

Fig. 1. CO (J=2–1) and (J=1–0) spectra observed towards heavily obscured OH/IR envelopes (histograms). The ^{12}CO spectra are from Heske et al., 1990. The continuous line is the best fit to the observations obtained with the superwind model (see text).

4.1. A physically small CO envelope

At some cutoff radius R_f, the CO abundance drops to zero, because of photodissociation or condensation onto grains, whichever occurs first. If R_f is small enough, the envelope is unresolved and its ^{12}CO (1–0) and (2–1) emissions are both optically thick.

The beam averaged brightness temperature of a line is then very close to the product of the beam dilution factor of the envelope with the excitation temperature at R_f, where the opacity abruptly drops from a value much larger than 1 to a value close to zero. Since CO(1–0) and CO(2–1) lines are expected to show very similar excitation temperatures, their intensity ratio is simply the ratio of the telescope HPBW at the corresponding frequencies. One thus expects an intensity ratio of 4, as observed.

It is possible to quantitatively reproduce the observed CO (2–1) and (1–0) emissions with a physically small model CO envelope. The kinetic temperature in the envelope is described by a power law, parametrized by the temperatures T_0 at an inner radius R_0 and T_f at the radius R_f where the CO abundance drops to zero (the temperature law index is then $\alpha = -\log(\frac{T_0}{T_f})/\log(\frac{R_f}{R_0})$).

The CO radiation emitted at radii of a few R_0 undergoes significant beam dilution and thus contributes negligeably to the observed emission. The model results are therefore insensitive to the choice of R_0 (as long as it remains small compared to the telescope resolution) and to T_0 (as long as it remains much larger than T_f). Of course, this would not hold true for higher rotational lines. In the following, we use R_0 = 10^{15} cm and T_0=1000K, but have checked that values of T_0 between 500K and 3000K give identical results.

In contrast, the lines intensities are very sensitive to the star's mass loss rate, $\dot{M}$, and to the outer cutoff radius R_f and temperature T_f.

In Table 4, we report the ranges of values of R_f and T_f which, for mass loss rates between 10^{-5} and 10^{-4} $M_\odot$ yr^{-1} (suggested by the IR data), reproduce the observed ^{12}CO (1–0) and (2–1) intensities towards OH127.8-0.0.

For mass loss rates higher than 10^{-5} $M_\odot$ yr^{-1}, the observed CO lines can only be reproduced with values of T_f which are too high to explain the CO abundance drop by condensation onto grains:CO is a very volatile molecule and only condensates onto grains at temperatures below 20K (Jura & Morris, 1985 ; Léger, Jura & Omont, 1985), i.e. at temperatures much lower than the

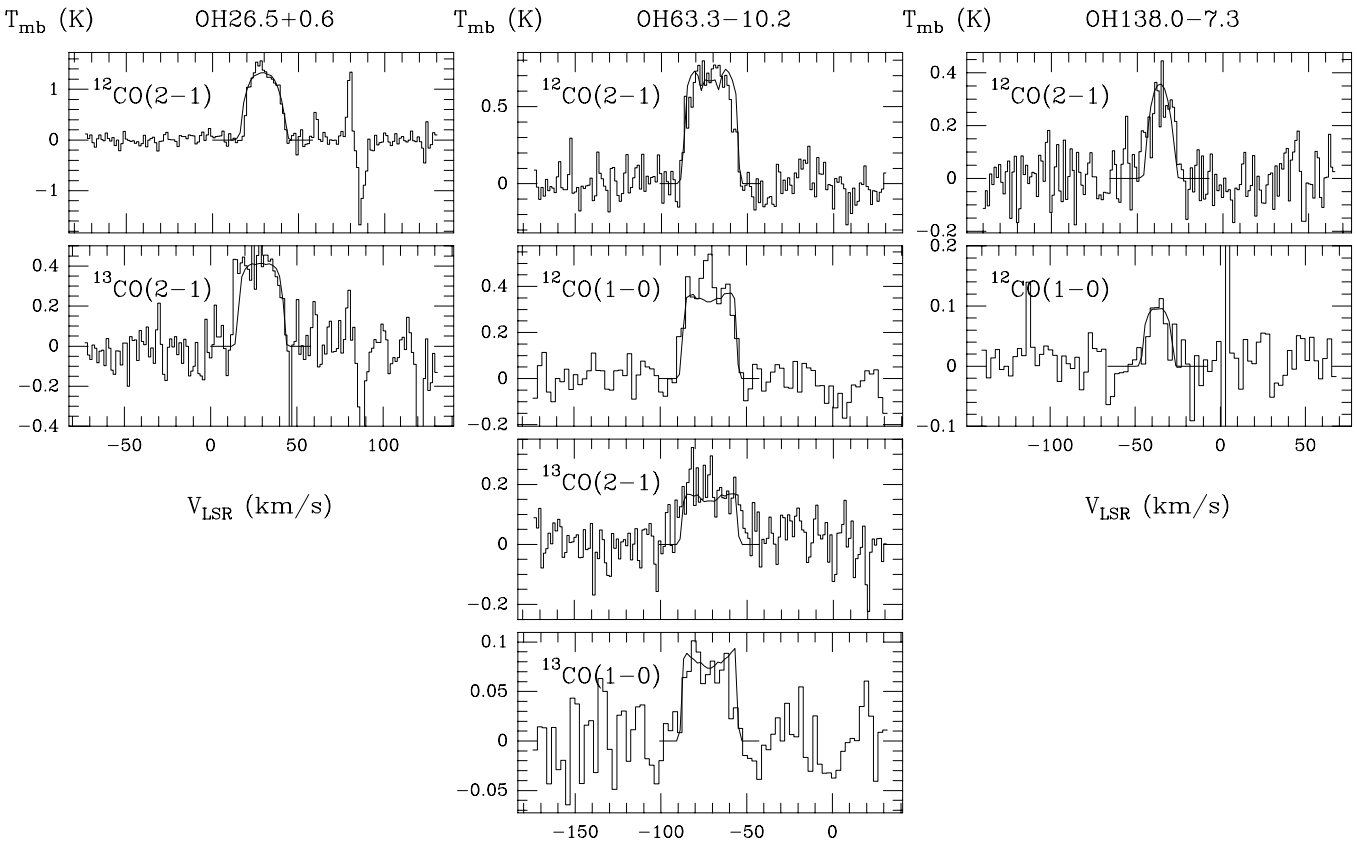

Fig. 2. The same as Fig. 1, except that, for OH63.3-10.2, the model corresponds to constant mass loss rate (see text).

Table 4. Parameters for small CO envelope model

$\dot{M}$ ($M_\odot$ yr^{-1})	R_f(10^{16}cm)	T_f (K)
10^{-4}	3–4	40–50
5.10^{-5}	4.5–5.5	30–40
10^{-5}	9–11	~ 30

values of T_f required to reproduce the CO lines intensities (see Table 4). Similarly, fit to the observed lines requires cutoff radii R_f which are too small to be explained by photodissociation: radii of $R_f \sim 10^{17}$ cm require mass loss rates smaller than 10^{-6}M$_\odot$ yr^{-1}, nearly independently of the local UV field (Mamon, Glassgold & Huggins (1988)). Such low $\dot{M}$ are clearly excluded by all models of far-IR emission from OH127.8-0.0 (HFOVH, Justtanont & Tielens, 1992 ; Justtanont et al., 1996 ; Schutte & Tielens, 1989).

4.2. A very cold outer envelope

Jura, Kahane & Omont (1988) have suggested that adiabatic cooling during expansion can cool the external parts of very thick circumstellar envelope to below 2.7K. If this happens, the CO molecules absorb the cosmic background radiation. In this very cold outer envelope, most CO molecules are in the ground state. Thus, they may absorb the (1–0) emission, but not the (2–1) emission arising from inner warmer layers. This tends to rise the (2–1)/(1–0) intensity ratio to the high value indicated by the observations.

Due to the Doppler shift, absorption in the very cold envelope would only affect part of the line profile and, in principle, could be diagnosed directly on a single spectrum. The available spectra are however too noisy for this to be feasible. To examine quantitatively whether such an envelope with a cold external layer can account for the observed CO lines intensity, we have used the same transfer model as above. The adopted kinetic temperature distribution was a power law for the inner part, with values of T_0 = 800 K at $R_0 = 10^{15}$ cm and T_f = 2 K at a break radius R_f, and was constant at 2 K from R_f out to the external radius, set to 10^{18} cm. We have explored the mass loss range 10^{-5} – 5 $\times 10^{-4}$ M$_\odot$ yr^{-1}. For mass loss rates below 10^{-4} M$_\odot$ yr^{-1} the cold outer layer is not thick enough to significantly absorb the (1–0) emission and the calculated (2–1)/(1–0) intensity ratio is lower than observed. For mass loss rates between 10^{-4} M$_\odot$ yr^{-1} and 5 $\times$ 10^{-4} M$_\odot$ yr^{-1}, very fine tuning of R_f is needed to reproduce the observed intensities (for this range of mass loss rates photodissociation radii are close to the adopted value of 10^{18} cm (Mamon et al., 1988)). In addition, the envelope parameters that reproduce the observed intensities turn out to be physically irrealistic: the mass loss between R_0

and 10^{18} cm integrates to a total envelope mass of at least 12 $M_\odot$, much larger than the maximum initial mass for an OH/IR star (6.5 $M_\odot$, Baud & Habing, 1983).

On different ground Groenewegen (1994), who has extended the analytic work by Jura, Kahane & Omont (1988) on the thermal structure of circumstellar envelopes, also concludes that a cold outer envelope is an unlikely explanation of the weak CO lines in OH/IR stars: photoelectric heating prevents cooling of the external envelope to below 2.7 K, except for unrealistically high mass loss rates.

4.3. a superwind phase

In agreement with previous works (Justtanont et al., 1996; Groenewegen, 1994), we conclude that it is impossible to reproduce the observed large ^{12}CO(J=2–1)/^{12}CO(J=1–0) ratio using a constant mass loss rate and any plausible temperature law in the envelope.

We examine now whether the assumption of a large and recent increase of the mass loss rate can provide an explanation for the observed CO line intensities. With such an assumption, the outer shell (which was expelled during the low mass loss rate phase) gives a negligible contribution to the CO emission. In contrast, the optically thick and still small inner shell, expelled by the star's so-called superwind, is responsible for the observed line intensities. This superwind phase was first suggested to occur in heavily obscured OH/IR stars by Baud & Habing (1983). It was also invoked by Heske et al. (1990) to explain why mass loss rates determined from CO with standard formulae are much lower in these stars than those inferred from far-IR flux (e.g. Jura, 1987) or from OH maser emission (Netzer & Knapp, 1987), which both originate closer to the star than CO emission.

4.3.1. Model parameters

We have experimented with various functional forms for the mass loss increase (linear increase or abrupt change). They produce equally good fits to the observations, and we are thus unable to constrain the shape of the transition between the two mass loss regimes. For the sake of simplicity, we assume in our modeling that the star has experienced two successive constant mass loss phases, a low rate one, $\dot{M}_l$, followed by a present-day high rate one, $\dot{M}_h$, with the same expansion velocity V_e = 13 km s^{-1}. The abrupt change in the circumstellar density law occurs at radius R_f, which corresponds to a superwind age $\tau_f = R_f/V_e$.

We find that the pre-superwind mass loss rate $\dot{M}_l$, is, to a large extent, arbitrary, as long as it remains small enough that the inner super-wind shell dominates the CO emission. Typically, this corresponds to $\dot{M}_l < 5 \times 10^{-6}M_\odot$ yr^{-1}. We thus adopt $\dot{M}_l$ = 10^{-6} M$_\odot$ yr^{-1} in the following. The envelope is truncated at an external radius of 10^{17} cm, close to the CO photodissociation radius calculated by Mamon et al., 1988 for a 10^{-6} M$_\odot$ yr^{-1} mass loss rate and an expansion velocity of 15 km s^{-1}. As expected, the results of the calculations are not very sensitive to this parameter. We have tried several superwind mass loss rates, $\dot{M}_h$ between 5 $\times 10^{-5}$M$_\odot$ yr^{-1} and 5 $\times$ 10^{-4}M$_\odot$ yr^{-1}, as suggested by the IR data.

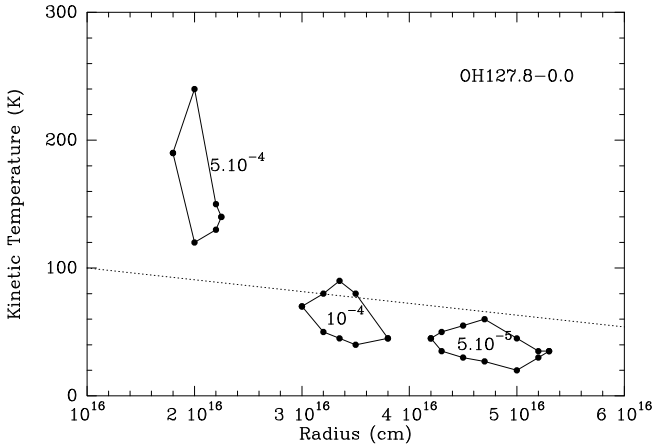

Fig. 3. Fraction of the $T_f \times R_f$ parameter space where the models reproduce the observed spectra of OH127.8-0.0 to within their one σ observational noise, for three values of the superwind mass loss rate. The dashed line represents the temperature law of Justtanont et al. (1996) for a mass loss rate of 10^{-4} M$_\odot$ yr^{-1} and an expansion velocity of 15.4 km s^{-1}.

The kinetic temperature in the envelope is described by a power law, parametrized by the temperatures T_0 = 1000 K at the inner radius R_0 = 10^{15} cm and T_f at the radius R_f, where the mass loss rate changes.

For each value of $\dot{M}_h$, T_f and R_f are adjusted to reproduce the ^{12}CO observations. Keeping the same values for these three parameters, the ^{12}CO/^{13}CO isotopic ratio is then adjusted to reproduce the ^{13}CO data.

4.3.2. Results

For realistic mass loss rates $\dot{M}_h$ between 5×10^{-5} and 5×10^{-4} M$_\odot$ yr^{-1}, fits to the observations to within the observational error bars can only be obtained in a small area of the $T_f \times R_f$ parameter space, as shown in Fig. 3.

The adjusted parameters are generally well constrained: over the explored range of mass loss rates, R_f (and therefore the age of the superwind) only varies by a factor of 2.5. The total mass in the superwind shell, M_{sw} is also constrained to the range $5 \times 10^{-2} M_\odot$ to a few $10^{-1} M_\odot$. The best determined parameter is however the carbon isotopic ratio which is independent of all other parameters and constrained to the range [3–3.5]. This is close to the equilibrium value for the CNO cycle. Table 5 summarizes the values of the free parameters required to reproduce the observed CO lines (i.e. a ^{12}CO(1–0) intensity between 0.14 K and 0.2 K and a ^{12}CO(2–1) intensity between 0.8 K and 1 K).

It can be noticed that, for mass loss rates of 5×10^{-5} and 10^{-4} M$_\odot$ yr^{-1}, the adhoc temperature laws we use to reproduce the observations are close to those derived for the mass loss rates of 10^{-4} M$_\odot$ yr^{-1} from the energy balance of the envelope (Justtanont et al., 1996). In contrast, for a (less realistic) mass

Table 5. Models of recent superwind for OH127.8-0.0

$\dot{M}_h$ $M_\odot$ yr^{-1}	T_f K	R_f 10^{16} cm	τ_f yr	M_{sw} 10^{-2} $M_\odot$	^{12}CO/^{13}CO
5.10^{-5}	20−60	4.2−5.3	1025−1290	5.1−6.5	3−3.5
10^{-4}	40−90	3.0−3.8	730− 925	7.3−9.3	3−3.5
5.10^{-4}	120−240	1.8−2.2	440− 550	22−27	3−3.5

Table 6. Mass loss rates derived from infrared data

OH	Gas Mass Loss Rates (10^{-4} $M_\odot$ yr^{-1}) $F_{60\mu m}$ [1]	$F_{25\mu m}/F_{12\mu m}$ [2]	S&T[3]	$\dot{M}_{dust}$ (10^{-6} $M_\odot$ yr^{-1}) J&T[4]
127.8 -0.0	1.28	0.92		2.0
30.1 -0.7	1.6	1.9	1.5	
104.9 +9.4	0.88	0.65		
26.5 +0.6	0.68	1.05	1.0	1.2
138.0 +7.3	0.5	0.29		
63.3 -10.2	0.09	0.15		

[1] Gas mass loss rates from the IRAS 60μm flux (Heske et al., 1990)
[2] Gas mass loss rates from the ratio of the IRAS fluxes at 25μm and 12μm (Heske et al., 1990)
[3] Gas mass loss rates from the near-infrared color temperature and the 10μm emission) (Schutte & Tielens, 1988)
[4] dust mass loss rates from infrared emission modeling (Justtanont and Tielens, 1992)

loss rate of 5×10^{-4} $M_\odot$ yr^{-1}, the energy balance temperature law drops much more rapidly than the ad hoc law used here to reproduce the CO intensities.

5. Modeling the other OH/IR envelopes

5.1. The "CO deficient" envelopes

5.1.1. Model parameters

We apply the superwind model developed for OH127.8-0.0 to the four other OH/IR stars with available CO(2–1) and CO(1–0) observations, and classified by Heske et al. as "deficient" in their CO emission.

As discussed in Sect. 4, nor the pre-superwind mass loss rate, nor the super-wind mass loss rate are severely constrained by the CO data: any value of $\dot{M}_l$ lower than 5×10^{-6} $M_\odot$ yr^{-1} and any value of $\dot{M}_h$ between 5×10^{-4} and 5×10^{-5} $M_\odot$ yr^{-1} lead to equally good fits.

We thus assume for all stars a sharp discontinuity in the mass loss rates, with a pre-superwind rate $\dot{M}_l = 10^{-6} M_\odot$ yr^{-1} and a superwind rate, $\dot{M}_h = 10^{-4} M_\odot$ yr^{-1}, typical of the mass loss rates derived by several authors from IR emission and listed in Table 6.

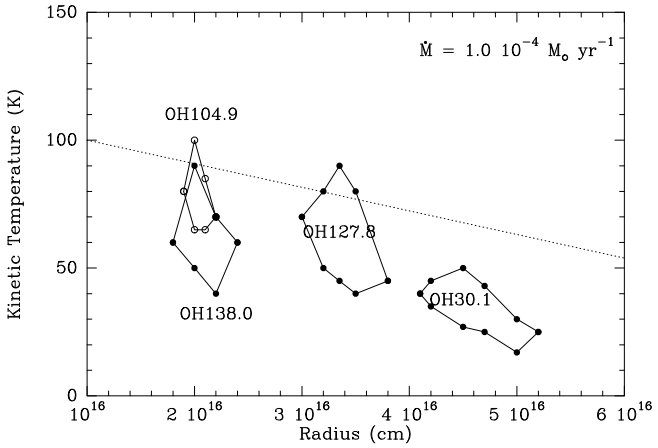

Fig. 4. Fraction of the $T_f \times R_f$ parameter space where the model CO spectra reproduce the observations of the four heavily obscured OH/IR envelopes, to within the one σ observational noise. The superwind mass loss rate is fixed at 10^4 $M_\odot$ yr^{-1}. The dashed line represents the temperature law of Justtanont et al. (1996) for this mass loss rate and an expansion velocity of 15.4 km s^{-1}.

As for OH127.8+0.0, the kinetic temperature is described by a power law with T_0=1000K at R_0 = 10^{15}cm, and T_f at a transition radius R_f. We have systematically explored the $R_f \times T_f$ parameter space to determine the area where a good fit to the observations is obtained for both ^{12}CO lines.

5.1.2. Observational constraints for individual stars

- *OH30.1 -0.7:* This star is the only one (OH127.8-0.0 excluded) for which the model parameters are constrained by a four line fit. The interstellar contamination of the line profiles is howevever quite substantial.
- *OH104.9 +9.4:* We have detected no ^{13}CO(1–0) emission towards this star. The ^{13}CO(2–1) line is very noisy and does not strongly constrain the ^{12}CO/^{13}CO abundance ratio.
- *OH26.5 +0.6:* Interstellar emission towards OH26.5 is strong and complex, so that we could not extract the contribution of its envelope from the observed ^{12}CO and ^{13}CO (J=1–0) spectra. The ^{12}CO(2–1) line alone does not constrain the temperature T_f, and we have used the temperature law derived by Justtanont et al.(1994) for a mass loss rate of 10^{-4} $M_\odot$ yr^{-1} and an expansion velocity of 15.4 km s^{-1}.
- *OH138.0 +7.3:* We have not observed the ^{13}CO lines towards this star.

5.1.3. Modeling results

The range of model parameters which reproduce the CO lines of the heavily obscured OH/IR stars are listed in Table 7 and displayed in Fig. 4.

The age of the superwind phase τ_f is determined to within better than a factor of two, and for all five stars it is a quite recent event (between 500 and 1000 years). It thus seems unlikely that the superwind phase lasts much longer than 1000 years, as

Table 7. Superwind models of the "CO deficient" OH/IR

Star	T_f K	R_f 10^{16}cm	τ_f (yr)	M_{sw} $10^{-2}M_\odot$	$^{12}CO/^{13}CO$
127.8 -0.0	40−90	3−3.8	730−925	7.3−9.3	3−3.5
30.1 -0.7	17−50	4.1−5.2	640−810	6.4−8.1	3−3.5
104.9 +9.4	65−100	1.9−2.2	390−450	3.8−4.5	3.5
26.5 +0.6	−	1.8−2.2	410−500	4−5	4−5
138.0 +7.3	40−90	1.8−2.4	600−800	6−8	

otherwise some examples of an old superwind phase would be observed.

The $^{12}CO/^{13}CO$ isotopic ratio is well constrained by the ^{13}CO line intensities. It is very similar and small (between 3 and 5) in all envelopes, close to the equilibrium value of the CNO cycle.

5.2. Less opaque OH/IR star

In contrast to the others, OH63.3 -10.2 belongs to the first group of OH/IR stars defined by HFOV: its mass loss rates determinations (Table 5) are lower ($\sim 10^{-5}M_\odot$ yr^{-1}) and the CO mass loss rate (computed with the Knapp and Morris (1985) formula) agrees well with the values derived from IR data.

All four ^{12}CO and ^{13}CO lines have been detected towards this envelope. We were able to fit them with a constant mass loss rate and a power law temperature distribution. The best fit was obtained for $\dot{M} = 9 \times 10^{-6}M_\odot$ yr^{-1} (in agreement with the mass loss rates calculated by Heske et al) and a power law temperature $T(r) = T_0(r(cm)/10^{15})^{-\alpha}$ with $T_0 = 1000K$ and $\alpha\sim0.7$, i.e. similar to the temperature law derived by Justtanont et al. (1996) for a mass loss rate of 1.0×10^{-4} $M_\odot$ yr^{-1} and an expansion velocity of 15.4 km s^{-1}. The isotopic $^{12}CO/^{13}CO$ abundance ratio required to fit the ^{13}CO lines is small, close to 5.

6. Discussion

6.1. The superwind phase

As discussed in detail in section 4, a recently increased mass loss rate provides the most simple and coherent explanation for (i) the apparent disagreement between mass loss rates derived from IR and CO data (ii) the "anomalously" high CO (J=2–1)/(J=1–0) intensity ratio observed for the heavily obscured "CO deficient" OH/IR stars. The infrared spectrum of these envelopes, which reflects their mass loss history, provides independent evidence for this superwind phase (Groenewegen, 1994): as longer wavelengths trace cooler dust and thus mass loss father from the star, a recent mass loss increase results in a flux excess at shorter ($\sim 25\mu m$) infrared wavelengths. With the benefit of hindsight, this can be discerned in the the results of Justtanont & Tielens (1992). Their constant mass loss rates models of the dust infrared emission of 24 OH/IR stars overestimate the long wavelength emission for five stars, which show the highest mass loss rates ($4.6 \times 10^{-7}M_\odot$ yr$^{-1} \leq \dot{M}_{dust} \leq 2.2 \times 10^{-6}M_\odot$ yr^{-1}) and which are all known (or likely) heavily obscured OH/IR stars.

6.2. The $^{12}C/^{13}C$ isotopic ratio and the mass of the OH/IR stars

Very low $^{12}C/^{13}C$ isotopic ratios (between 3 and 5) may be explained by hot bottom burning at the base of the convective envelope. This requires a temperature of at least 80 $\times 10^6$ K, which is only reached in massive stars ($M \geq 5M_\odot$), and at the end of their AGB phase (Boothhroyd, Sackmann & Ahern, 1993). These theoretical calculations also predict high luminosities ($L \geq 3 \times 10^4L_\odot$).

The luminosity of OH127.8, OH26.5 and OH138.0 calculated with the bolometric correction of Van der Veen & Breukers (1989) (respectively $(5.7 \pm 2.3)\times10^4L_\odot$, $(2.2 \pm 0.8)\times10^4L_\odot$ (Van langevelde et al. 1990) and $2.6 \times 10^4L_\odot$ (Heske et al. 1992)) are consistent with the theoretical calculations of Boothroyd et al. (1993), considering that they are not corrected for the interstellar extinction (in addition OH138.0 is a known variable). No phase lag distances are available for OH63.3 nor OH30.1, so that their luminosities are unknown (the distances reported in Table 3 assume luminosities of 10^4 $L_\odot$). The only star with a measured luminosity that could be smaller than the theoretical limit of $3 \times 10^4L_\odot$ is OH104.9 +9.4: when correcting the IRAS fluxes at $12\mu m$ and $25\mu m$ (Hermann, Burger & Penninx (1986) with the interstellar correction of Milne & Aller (1980) and the interstellar extinction curve of Becklin et al.(1978) before applying the bolometric correction of Van der Veen & Breukers (1989), we obtain a luminosity of $1.4 \times 10^4L_\odot$. This however ignores stellar variability which, together with the significant distance uncertainty, could bring OH104.9 +9.4 into agreement with the theoretical calculations.

6.3. Evolutionary status

According to their $^{12}C/^{13}C$ isotopic ratios, the OH/IR stars in both groups are relatively massive stars ($M \geq 5M_\odot$). This conclusion agrees with the standard view that the OH/IR stage is the last phase of massive (5–8$M_\odot$) star evolution before a planetary nebula forms. The presence or absence of a superwind and, if significant, a marginally higher $^{12}C/^{13}C$ ratio in the thinner envelopes, are evidence for slightly different evolutionary stages. The OH/IR stars with less opaque envelopes approach the end of their AGB phase, as shown by their low $^{12}C/^{13}C$ isotopic ratio, but they have not yet reached the final envelope ejection stage. The heavily obscured OH/IR stars are in a more advanced stage and have begun to eject their envelope in a superwind. This terminal phase lasts for $\sim$ 1000 yr, with mass loss rates of $\sim 10^{-4}M_\odot$ yr^{-1}.

As we only have data for a single OH/IR envelope of the first group, this scenario clearly needs to be confirmed by additional observations. It would, in particular, be interesting to establish whether the small difference in the $^{12}C/^{13}C$ ratios measured for the two types of OH/IR envelopes is significant (5 for OH63.3-10.2, 3 to 3.5 for the superwind OH/IR stars).

The derived superwind lifetime is consistent with the observed number of heavily obscured OH/IR stars. Baud & Habing (1983) have estimated the lifetime of the superwind phase from the OH luminosity function and the assumption that the OH/IR stars showing very strong OH emission experience a superwind. They obtain a typical lifetime of 10^2–10^3 yr. Statistical arguments and modeling of CO emission thus produce consistent estimates of the superwind duration.

Interferometric CO observations should be able to resolve the inner CO envelope and would provide a direct check of the existence of two mass loss regimes in the envelope. They would strongly constrain the duration, mass loss rate, and expansion velocity during the superwind phase. They might be able to probe the shape of the transition between the two regimes.

Acknowledgements. It is a pleasure to thank Robert Lucas, who has kindly let us use his radiative tranfer code, and Kay Justtanont for communicating results before publication. The computations presented in this paper were performed at the "Centre de Calcul Intensif de l'Observatoire de Grenoble".

References

Baud B., Habing H. J., 1983, A&A 127, 73
Becklin E. E., Matthews K., Neugebauer G., Willner S. P., 1978 ApJ 220, 831
Boothroyd A. I., Sackmann I. J., Ahern S. C., 1993 ApJ 416, 762
Gehrz R. D., Kleinmann S. G., Mason S., Hackwell J. A., Grasdalen G. L., 1985 ApJ 290, 296
Groenewegen M.A.T., 1994, A&A 290, 544
Herman J., Burger J. H., Penninx W. H., 1986 A&A 167, 247
Herman J., Habing H.J., 1985 A&A Suppl. Ser 59, 523
Heske A., Forveille T., Omont A., Van der Veen W. E. C. J., Habing H. J., 1990 A&A 239, 173
Jura M., 1987, ApJ 313, 743
Jura M., Kahane C., Omont A., 1988, A&A 201, 80
Jura M., Morris M., 1985, ApJ 292, 487
Justtanont K., Skinner C. J., Tielens A. G. G. M., Meixner M., Baas F., 1996, ApJ 456, 337
Justtanont K., Tielens A. G. G. M., 1992, A&A 389, 400
Kahane C., Jura M., 1994, A&A 290, 183
Knapp G. R., Morris M., 1985, ApJ 292, 640
Leger A., Jura M., Omont A., 1985, A&A 144, 147
Mamon G. A., Glassgold A. E., Huggins P. J., 1988, ApJ 328, 797
Milne D. K., Aller L. H., 1980 AJ 85, 17
Netzer N., Knapp G. R., 1987, ApJ 323, 734
Sahai R., 1990, ApJ 362, 652
Schinke R., Engel V., Buck U., Meyer H., Diercksen G.H.F., 1985, ApJ 299, 939
Schutte W. A., Tielens A. G. G. M., 1989 ApJ 343, 369
Van der Veen W. E. C. J., Breukers R. J. L. H., 1989 A&A 213, 133
Van der Veen W. E. C. J., Olosson, H., 1989 in *From Miras to Planetary Nebulae: which path for stellar evolution ?* Eds. M.O. Mennessier and A. Omont
Van Langevelde H. J., Van der Heiden R., Van Schooneveld., 1990, A&A 239, 193

This article was processed by the author using Springer-Verlag LaTeX A&A style file *L-AA* version 3.